Soil Microbial Functional Succession Over One Year of Human Decomposition

Allison R. Mason[1], Lois S. Taylor[2], Naomi E. Gilbert[1], Steven W. Wilhelm[1], Jennifer M. DeBruyn[1,2*]

[1]Department of Microbiology, University of Tennessee-Knoxville, 1311 Cumberland Avenue, Knoxville, 37996.

[2]Department of Biosystems Engineering and Soil Science, University of Tennessee-Knoxville, 2506 E.J. Chapman Drive, Knoxville, 37996.

*Corresponding author(s). E-mail(s): jdebruyn@utk.edu;

Abstract

During terrestrial vertebrate decomposition, host and environmental microbial communities work together to drive biogeochemical cycling of carbon and nutrients. These mixed communities undergo dramatic restructuring in the resulting decomposition hotspots. To reveal the succession of both the active microbial members and the metabolic pathways they use, we generated metatranscriptomes from soil samples collected over one year from below three decomposing human bodies. Soil microbes increased expression of "heat shock" proteins in response to decomposition products changing physiochemical conditions (*i.e.*, reduced oxygen, high salt). Increased fungal lipase expression implicated fungi as key decomposers of fat tissue. Expression of nitrogen cycling genes was phased with soil oxygen concentrations: during hypoxic soil conditions, genes catalyzing N-reducing processes (*e.g.*, hydroxylamine to nitric oxide and nitrous oxide to nitrogen gas during reduced oxygen conditions) were increased, followed by increased expression of nitrification genes once oxygen diffused back into the soil. Increased expression of bile salt hydrolases implicated a microbial source for

the high concentrations of taurine typically observed during vertebrate decomposition. Collectively, microbial gene expression profiles remained altered even after one year. Together, we show how human decomposition alters soil microbial gene expression, revealing both ephemeral and lasting effects on soil microbial communities.

Keywords: Human Decomposition, Microbial Succession, Metatranscriptomics, Soil Microbial Ecology

Introduction

Soil microbial communities are important drivers of ecosystem processes in terrestrial environments. Many soil microbes are decomposers that degrade complex organic matter and drive nutrient cycling in terrestrial ecosystems. Environmental disturbances can impact the presence and/or activity of soil microorganisms involved in these cycles, ultimately affecting nutrient availability and greenhouse gas emissions, such as CO_2 and N_2O [1, 2]. Vertebrate death and subsequent carcass deposition in terrestrial ecosystems is one disturbance resulting in the deposition of large quantities of organic C and N [3–10], along with other elements (P, K, S, *etc*) [11], which collectively contribute to microbially-mediated biogeochemical cycling. In addition to this, changes in pH, temperature, and fluctuations in soil oxygen provide abiotic filtering further impacting microbial metabolic strategies [7–9, 11–13]. Vertebrate decomposition also results in mixing of host and environmental microbes: the animal's microflora are flushed into the soil along with decomposition products where they further contribute to decomposition processes (*e.g.*, organic nitrogen mineralization) [14].

While C and N transformations have been documented during decomposition, the functional response of microbes and their roles in nutrient cycles remain unclear. The composition and structure of decomposition-impacted soil microbial communities have been investigated using sequencing of marker genes amplicons (*i.e.*, 16S rRNA, 18S

rRNA, ITS). This has allowed for the identification of changes in microbial biodiversity and taxonomic succession in response to vertebrate decomposition, revealing patterns that include increases in the anaerobic taxa *Firmicutes* and *Bacteroidetes* [15]. However, few studies have integrated soil biogeochemistry with microbial community composition, which can further help to describe microbial ecology in these decomposition systems. Taylor et al. (2024) [13] showed that fungal community shifts were linked to changes in soil dissolved oxygen, highlighting interactions between soil microbes and changes in the surrounding environment. While insightful for making potential connections between taxa and environment, these analyses do not inform which taxa are active members of the community, which functional pathways/genes are expressed, and how these pathways facilitate decomposition processes.

RNA sequencing (*i.e.*, metatranscriptomics) and metabolomics can be used to investigate microbial community functional succession during decomposition. They can identigy how ecological functions, including C and N cycling, are impacted by decomposition events in terrestrial ecosystems. To date, applications of metatranscriptomics to vertebrate decomposition samples have been limited to internal host communities [16, 17]: Burcham et al. (2019) [16] revealed differential expression of amino acid and carbohydrate metabolism in the heart during mouse decomposition, while Ashe et al. (2021) [17] documented taxonomic shifts in gene expression of oral microbial communities during human decomposition.

We expected that the impacted soil microbial community, which includes a mix of host and environmental taxa, would also have altered gene expression profiles, given the release of decomposition byproducts into the soil during terrestrial decomposition. We previously assessed the decomposition-impacted soil metabolome [18], demostrating a prevalence of amino acids and suggesting upregulation of organic nitrogen metabolic pathways. Additionally, DeBruyn et al. (2021) [18] showed the soil metabolome was

surprisingly still altered compared to starting conditions at the end of that 21-week study, suggesting long-term impacts of decomposition on soil microbial functioning.

Here, we investigated soil microbial gene expression during a one-year period of human decomposition. The overarching goal of this work was to assess the effects of vertebrate decomposition on ecosystem function by characterizing community-level shifts in soil microbial function. We hypothesized that: (i) gene expression would shift over time as resources were consumed and transformed and soil chemical and physical conditions changed due to the influx of decomposition products during soft tissue degradation [8, 9, 18]; (ii) gene expression for enzymes involved in nitrogen cycling would be altered, as changes in nitrogen pools have been previously described in decomposition soils [8]; (iii) expression of genes involved in lipid metabolism would increase, as lipids from the body entered the soil during decomposition and previous studies identified lipolytic organisms in decomposition soils [12, 19]; (iv) microbial expression profiles in the impacted soil would remain altered even after a year, as previous studies have shown that community composition [20, 21] can remain altered longer than a year. We analyzed metatranscriptomes of soil samples collected at six key timepoints over one year of human decomposition to determine the identity of active populations and the expression of genes and pathways relevant to the enhanced biogeochemical cycling observed in decomposition hotspots. We compared gene expression between decomposition timepoints and control soils that were unexposed to decomposition products to identify functions or functional pathways of interest. We show: (i) decomposition shifts soil microbial community gene expression, with the effects still measurable after one year; (ii) expression of genes related to stress response are elevated in decomposition soils; (iii) expression of genes encoding triacylglycerol lipase differed between fungi (increased) and bacteria (decreased); (iv) evidence for phased nitrification and denitrification, driven by changes in soil dissolved oxygen; (v) evidence for organic

sulfur processing (taurine) via bile salt hydrolases. This direct assessment of function expands the fudamental understanding of terrestrial vertebrate decomposition, providing insight into pathways of biogeochemical cycling within these hotsopts.

Results

Soil Physiochemistry

Soil chemistry was altered in response to the presence of a decomposing human cadaver, with multiple parameters still impacted after one year [13]. Generally, soil pH decreased and remained low in decomposition soils of all but one individual. Soil electrical conductivity (EC) increased in response to decomposition, remaining elevated through approximately day 58 before gradually decreasing throughout the remainder of the study (Supplementary Fig. 1). Respiration (evolved CO_2) increased by an order of magnitude beginning at day 12, which corresponded to a reduction in soil dissolved oxygen (DO) to 29% - 48.9%. Ammonium concentrations increased 78-fold, reaching maximum concentrations between days 12 and 58. This was followed by decreased ammonium and increased nitrate concentrations at day 86, with nitrate concentrations reaching a maximum at day 168 (Supplementary Fig. 1).

Microbial gene expression in response to human decomposition

Gene expression profiles in decomposition-impacted soils shifted away from controls and day zero samples as decomposition progressed (Fig 1A). Expression was most different from controls on study days 58, 86, 168 (Supplementary Fig. 2), before returning toward control conditions on study day 376. After one year of decomposition, soil gene expression profiles had not returned to pre-decomposition conditions, as evidenced by their clustering away from controls and day zero samples in the MDS plot (Fig 1A).

Some correlations were observed between gene expression shifts and soil physiochemical data at decomposition timepoints. Canonical correspondence analysis (CCA) was used to constrain gene expression data with soil physiochemical data (Fig 1B). CCA1 and CCA2 explained 29.2% and 18.1% of the variance in gene expression, respectively. Transcript profiles at day 12 were associated with an increase in soil carbon to nitrogen ratio (C:N). Gene expression profiles at days 58 to 86 were positively correlated with increased soil temperature, EC, and evolved CO_2, while study day 168 was associated with elevated levels of soil NO_3. Further, Permutational Analysis of Variance (PERMANOVA) revealed that internal accumulated degree hours (ADH) ($p = 0.001$), soil temperature ($p = 0.039$), pH ($p = 0.033$), and EC ($p = 0.031$) significantly explained some of the variation in gene expression profiles ($p < 0.05$). No other soil chemical variables were significant at $\alpha = 0.05$ (Supplementary Table 1).

Overall, decomposition changed soil gene expression profiles over the one-year study relative to control soils. Differential expression analysis between decomposition and control soils identified 7,047 down-regulated and 38,425 up-regulated genes. Gene transcripts that were associated with control soils belonged to a wide variety of clusters of orthologous genes (COG) functional categories. Specifically, the top 20 genes whose expression was higher in control soils belonged to ten unique COG categories, including signal transduction mechanisms, transcription, and those of unknown function. In contrast, the top 20 genes whose expression was higher in decomposition soils only fell into four COG categories (Supplementary Fig. 3 A): 1) post-translational modification, protein turnover, and chaperones; 2) energy production and conversion; 3) cell motility; and 4) carbohydrate transport and metabolism. The most common COG category represented in decomposition soils (80% of the top 20 genes) was post-translational modification, protein turnover, and chaperones. Within this category, several heat shock stress response genes were identified, including clpB, dnaK, groL2, SSA2, HSP82, and clpB (Supplementary Table 2). Further investigation of these genes

over time shows that their expression increased, typically reaching maximum transcript levels around study days 58 and 86 (Fig 2). This corresponded to elevated soil temperatures below decomposing bodies between study days 12-80, with soil temperatures increasing to approximately 43°C [13], as well as maximum soil EC and minimum dissolved oxygen measurements between days 12 and 58 (Supplementary Fig. 1).

Taxonomy associated with top differentially expressed gene transcripts also differed between control and decomposition soils. The top 40 most significant differentially expressed gene transcripts in decomposition soils were associated with Fungi, *Actinobacteria*, and *Xanthomonadales*, while gene transcripts in controls were associated with *Acidobacteria*, *Cyanobacteria*, *Proteobacteria* (α, δ, γ), and *Planctomycetes* (Supplementary Fig. 3 B). The greatest number of differentially expressed genes relative to control samples was observed at day 86, where we saw 145,460 and 124,883 up- and down-regulated genes, respectively.

Temporal gene expression shows shifted in decomposer functions

Differential expression analysis between sequential study days revealed which genes were altered during decomposition time. The top ten transcripts that changed in representation (increased/decreased), determined by the lowest p-values from differential expression analysis, are reported in Supplementary Table 3 and Fig 3.

Expression of genes annotated with the COG categories cell wall/membrane/envelope biogenesis, inorganic ion transport and metabolism, and carbohydrate transport and metabolism increased proportionally from day 0 to 12. In contrast, expression of secondary metabolite biosynthesis, transport, and catabolism genes decreased during this period (Fig 3A). Transcripts from *Bacilli* and *Clostridia* increased, while transcripts from *Actinobacteria* decreased between study days zero and 12 (Fig 3).

Between days 12 and 58, 90% of the top 10 upregulated genes were associated with the translation, ribosomal structure and biogenesis COG and all were taxonomically associated with *Betaproteobacteria* (Fig 3A,B). Many of these genes were annotated as ribosomal protein large (RPL), involved in ribosomal binding. Genes across multiple COG categories with taxonomic associations to *Bacilli* and *Clostridia* decreased between study days 12 and 58, six of which were transcripts that previously increased between days zero and 12 (Fig 3B, Supplementary Table 3).

Multiple transcripts associated with the energy production and conversion COG, as well as transcripts annotated with the COGs inorganic transport and metabolism, and translation, ribosomal structure and biogenesis, increased between days 58 and 86 (Fig 3A). Two of the upregulated energy and production and conservation transcripts were associated with cytochrome c oxidase subunits in *Betaproteobacteria*, while another was annotated as *hao*, encoding the enzyme hydroxylamine dehydrogenase which is involved in conversion of hydroxylamine to nitrite during nitrification (Supplementary Table 3). Further investigation into hydroxylamine dehydrogenase showed a significant increase in *hao* transcripts at day 86 followed by subsequent decreases at days 168 and 376 ($F = 4.183$; $p = 0.02$). This increase corresponded to decreased soil ammonium levels and subsequent accumulation of nitrate (Supplementary Fig. 1). Half of the topmost downregulated genes between days 58 and 86 were not assigned to a COG (*i.e.*, unclassified) or were of unknown function.

Differential expression comparing study days 86 with 168 and 168 with 376 identified genes across a variety of functional categories, with many unclassified in the COG database or with unknown function (Fig 3A). Expression of carbohydrate transport and metabolism genes associated with *Bacilli* decreased between day 168 and 376. *Acidobacteria* transcripts increased in decomposition-impacted soils between study day 168 and 376, but were not associated with any single COG category (Fig 3B).

Organic carbon metabolism

We expected to observe increased expression of lipid metabolizing genes during active and advanced decomposition as microbes degraded lipids deposited in the soil [19]. Therefore, we investigated changes in triacylglycerol lipase (enzyme commission number: 3.1.1.3) gene transcription in our soils. Generally, lipase transcripts decreased as decomposition progressed (HLM F = 6.564, $p < 0.001$), however we also observed a significant interaction between study day and taxonomic annotation (F = 8.786; $p < 0.001$). Specifically, lipase gene transcripts annotated as bacteria decreased with decomposition time (F = 10.392; $p = 0.001$), while fungal lipase transcripts increased, reaching a maximum at study day 58 (F = 4.509; $p = 0.015$) (Fig 4).

Nitrogen- and sulfur compound transformations

Expression of nitrogen cycling genes was impacted in response to human decomposition. Due to the detection of hydroxylamine oxidoreductase (*hao*) transcripts in our differential expression analysis, and our hypotheses predicting changes to nitrogen transformation processes, the expression of genes encoding common enzymes involved in nitrogen cycling (*nifH*, *nirB*, *nirK*, *norB*, *nosZ*, *nrfA*, *nxrA*, and *amoA*) were assessed using their enzyme commission numbers (Fig 5A,B). *nifH*, encoding a subunit of nitrogenase which is involved in nitrogen fixation, displayed little to no changes in gene expression between control and decomposition soils. Transcripts for two genes encoding enzymes contributing to the last two steps of denitrification, *norB* (nitric oxide reductase) and *nosZ* (nitrous oxide reductase), increased between study days 12 and 86, and decreased at study day 168 before increasing again at day 376. In contrast, expression of genes encoding nitrate reductase, *narG*, and NO-forming nitrite reductase, *nirK*, remained low until day 376 when transcripts for both genes increased. As noted above, expression of *hao*, encoding hydroxylamine dehydrogenase, increased at study day 86 before decreasing at remaining timepoints (Fig 3A, Fig 5B). Expression

of *amoA*, encoding a subunit of ammonia monooxygenase, and *nxrA*, encoding a subunit of nitrite oxidoreductase, which are involved in nitrification, changed in response to decomposition. *amoA* transcripts initially decreased at day 12, remaining reduced until study day 376. Similarly, abundance of genes that encode for enzymes involved in dissimilatory nitrate reduction, *nirB*, and *nrfA*, was low for the first 168 days, with *nrfA* expression increasing at day 376 (Fig 5B).

Expression of genes involved in metabolism of nitrogen and sulfur-containing compounds were also impacted by human decomposition. Specifically, four of the top ten genes whose expression decreased at day 12 were related to taurine metabolism, with their annotations associated with *tauD*, encoding taurine dioxygenase. (Supplementary Table 3). Further investigation into *tauD* showed that mean expression of these genes decreased steadily over one year, beginning at day 12 (Fig 6B); however, *tauD* expression in response to human decomposition was variable across taxonomic associations. Most *tauD* transcripts were associated with *Gammaproteobacteria*, *Actinobacteria*, *Betaproteobacteria*, *Alphaproteobacteria*, and fungi. While a majority of the *tauD* gene queries displayed reduced expression over time, expression of fungal-associated and a few *Betaproteobacteria*-associated *tauD* genes increased at day 58 (Supplementary Fig. 4). Sources of taurine in the human body include taurine absorbed from the diet and taurine produced from anaerobic microbial deconjugation of bile salts via bile salt hydrolase (BSH) enzymes [22]. Therefore, we examined expression for genes encoding BSH enzymes in decomposition soils. Expression of these genes was elevated at days 12, 58, and 86 before converging toward pre-decomposition levels at days 168 and 376 (Fig 6A). Hierarchical liner mixed effects (HLM) models showed that both *tauD* (HLM $F = 7.356$, $p = 0.002$) and BSH ($F = 13.768$, $p < 0.001$) gene expression was significantly different over time (Fig 6A,B).

Discussion

The goal of this study was to assess microbial gene expression in soils responding to human decomposition. Metatranscriptomics were applied to soil samples collected over one year from below three decomposing human bodies. From this, we found that microbial gene expression reproducibly shifted over time. Additionally, we showed that gene expression profiles had not recovered to pre-decomposition conditions after one year. Comparison of control and decomposition expression profiles revealed that heat-shock proteins were elevated in response to decomposition. We also described expression patterns between decomposition timepoints, noting changes in functional gene categories at certain timepoints, in particular with respect to lipid, nitrogen and sulfur metabolism.

Decomposition impacted soil community gene expression, for at least one year

Gene expression profiles remained altered after one year of decomposition. It is unclear if soil microbial communities, in terms of gene expression profiles, have reached a new steady state as a result of decomposition, or if they would eventually return to pre-decomposition conditions. The soil pH, EC, NH_4^+, NO_3^-, and total nitrogen (TN) exhibited differences (although not statistically significant) in these soils following a year of decomposition, however bacterial and fungal community structures, as assessed by rRNA amplicon libraries, were still altered [13]. This indicates that decomposition can continue to structure microbial communities and impact their function for extended periods of time. While nutrient pools and communities both demonstrate less rapid change at later time points in the study, there is no evidence suggesting an arrival at a steady-state post-disturbance microbial community within our study. In some studies, human decomposition can result in elevated carbon and nutrients (organic nitrogen, ammonium, nitrate, and phosphate) for longer than a year [3], suggesting

decomposition events have long-lasting effects on the local ecosystem. Together, this has implications for terrestrial ecosystem processing (*e.g.*, nutrient cycling, emission of greenhouse gasses, etc.), as we show that decomposition alters functional metabolism pathways within soil microbial communities. It is clear that extended sample collections beyond a single year are needed to address how long microbial communities are effected, and whether there is a return to the original state or some new altered community condition.

Bacteria, fungi, and archaea were all represented by expressed genes throughout decomposition, suggesting that members of all three domains have the potential to contribute to decomposition processes and nutrient cycling. While a majority of annotated transcripts were identified as bacterial, fungal transcripts were the second most abundant group. Fungal transcripts made up almost half (*e.g.*, seven of the top fifteen) of the significantly differentially expressed genes associated with decomposition-impacted soils. Additionally, with respect to expression shifts between decomposition timepoints, fungal transcripts were among the topmost upregulated genes at study day 86. This is not surprising as fungi are key decomposers, involved in the degradation of organic matter in terrestrial ecosystems [23]. It was interesting to see an increase in certain fungal transcripts, such as lipase, at study days 58 and 86 when soil oxygen began to recover. We would expect lipids to enter the soil as tissues are broken down during decomposition, so we were surprised to see bacterial lipase genes decrease during decomposition. This suggests that microbial activity in decomposition soils may be constrained by the changing chemical environment, potentially altered oxygen levels in the case of bacterial lipase gene expression. Prior work with these same soils showed that soil oxygen concentration was a key driver of changes in both bacterial and fungal community composition [13].

Increased stress responses during decomposition

Soil microbial communities expressed stress response genes in response to human decomposition. Differential expression analysis identified increased expression of multiple heat shock proteins associated with the taxa *Xanthomonadales*, *Actinobacteria*, and fungi. Upon further investigation, expression of these genes increased through day 58 and remained high for the remainder of the year. Soil temperature was elevated relative to controls between study days 8 and 80, with maximum temperatures >40°C, while soil electrical conductivity increased up to 663 µS/cm (16X higher than background) through day 58 before slowly decreasing through the remainder of the study. Soil electrical conductivity correlates with ionic strength and can be an indicator of increased salinity [24]. With regard to vertebrate decomposition, early elevated conductivity in impacted soils is attributable to sodium (Na), potassium (K), and ammonium (NH_4) [8–11, 13]. As a result, we would expect these microbes to be experiencing both heat and osmotic stress during this period. Prior work has observed increased heat shock gene expression during salt stress in paddy soils [25] and the presence of both heat and osmotic stress genes in desert soils along a salt gradient [26], suggesting saline conditions can alter the expression of heat and/or osmotic stress genes. In our study we observed the stress response within soil microbial communities was stimulated during human decomposition. At this time, however, it is unclear if expression of these genes is in response to heat stress alone, or in combination with osmotic stress.

Increased expression of fungal lipase genes during decomposition

Human fat tissue contains lipids that are broken down during decomposition. Therefore, we assessed expression of triacylglycerol lipase genes in decomposition soils. Our results show that expression of triacylglycerol lipase genes was altered in response

to decomposition, and these shifts differed between bacterial and fungal transcripts. Specifically, bacterial triacylglycerol lipase transcripts decreased in response to decomposition, while fungal triacylglycerol lipase transcripts increased. Further, expression of these genes corresponded to changes in relative abundance of the fungal classes *Saccharomycetes*, *Sordariomycetes*, and *Eurotiomycetes* [13]. These fungi have been previously associated with decomposition soils [27, 28] and are known to contain triacylglycerol lipase genes in their genomes [29, 30], suggesting that they play a role in lipid degradation in decomposition soils.

Our observation of an overall decrease in triacylglycerol lipase transcripts contrasts with previous work by Howard et al. (2010) [19], who observed increased gene copy number of Group 1 lipase genes via qPCR during swine decomposition. Fatty acid composition differs in human compared to pig tissue [31], potentially altering the lipids profile available for microbes, leading to differences in decomposition products within the soil [18]. These products can then directly or indirectly alter community composition and/or activity of functional proteins via substrate availability or the chemical environment. Further, decomposition of humans and pigs resulted in increased pH in soils below pigs, and decreased pH below humans [18]. Altered pH and soil chemistry could result in a different functional potential and/or gene expression in decomposition-impacted soils. Many triacylglycerol lipases have a pH optimum that is neutral to basic [32–34], so cells may be decreasing expression under acidic conditions in human decomposition soils. Availability of lipid species and changes to pH may select for taxa that favor these substrates/pH conditions; for example, Mason et al. (2022) [12] suggested the abundance of the fungal taxa *Saccharomycetes* was related to antemortem BMI due to relative proportions of fat and muscle tissue.

Evidence for phased denitrification and nitrification

The human body is a concentrated source of nitrogen that is released into the surrounding soil during decomposition. Expression of common marker genes for nitrogen cycling was altered in decomposition soil and suggested nitrogen transformations during human decomposition are driven by soil oxygen concentrations with hydroxylamine as an important intermediate. We observed low or reduced expression of the nitrification genes *nxrA* and *amoA* between days 12 and 86, during a period when oxygen was reduced to 39% - 85%. This was concomitant with an accumulation of ammonium, which reached a maximum on day 12, and low nitrate conditions indicating that nitrification was inhibited. This period of reduced soil oxygen constraining nitrification was also described in a decomposition experiment with beaver carcasses Keenan et al. (2018) [8].

We observed increased gene expression for the enzyme hydroxylamine dehydrogenase (HAO) at day 86 while oxygen was reduced (~85%). This corresponded to simultaneous increases in expression of genes encoding nitric oxide reductase (*norB*) and nitrous oxide reductase (*nosZ*). Traditionally HAO has been thought to process hydroxylamine to nitrite during nitrification, while NorB and NosZ are enzymes involved in the last two steps of denitrification converting nitric oxide (NO) to dinitrogen gas (N_2). However, recent work suggested hydroxylamine can be converted to nitric oxide (NO), and can interact with multiple phases of the nitrogen cycle [35]. Even though *amoA* expression was shown to decrease during reduced oxygen conditions, *amoA* transcripts were still present and likely able to convert ammonium to hydroxylamine as soil oxygen was not completely depleted during decomposition. Additionally, a previous study reported that the growth of the ammonia oxidizing bacteria *Nitrosomonas europaea* under anoxic conditions lead to accumulation of hydroxylamine in a chemostat bioreactor [36], suggesting anaerobic ammonium oxidation (anammox) may also be occurring in decomposition soils. However, we did not observe increases in *nirK*

expression, which might suggest conversion of nitrite to NO for use in the anammox pathway. NO produced via HAO activity may be used for anammox in these soils; however, the role of hydroxylamine as an intermediate in anammox is still debated [35]. Therefore, our current hypothesis is that hydroxylamine accumulates under anaerobic conditions during decomposition, which can then be converted to NO by HAO. This NO would then be present for anaerobic denitrifying bacteria to convert to nitrous oxide (N_2O) by NorB and finally to N_2 by NosZ. Keenan et al. (2018) [8] noted a brief increase in N_2O emissions, which suggests denitrification was occurring during this phase of reduced soil oxygen concentrations.

As soils fully reoxygenated by day 168, we observed increased expression of genes encoding enzymes involved in aerobic nitrification, *amoA* and *nxrR*. Nitrification is an oxygen-dependent process which would convert accumulated ammonium to nitrate; the increase in nitrate concentrations may then serve as a substrate for denitrification. We observed increased expression of marker genes encoding all four enzymes in the complete dissimilatory denitrification pathway (*narG*, *nirK*, *norB*, and *nosZ*) at day 376. Increased expression of nitrification and denitrification marker genes is consistent with the accumulation of nitrite, nitrate, and N_2O after oxygen is reintroduced to soils described in Keenan et al. (2018) [3, 8]. Together, gene expression patterns in our study provide further insight into nitrogen transformations in during vertebrate decomposition, suggesting an important role of hydroxylamine.

Increased expression of bile salt hydrolases

Sulfur is present in various organic molecules, including taurine, a sulfur- and nitrogen-rich compound involved in bile acid formation [22]. Taurine in the human body can be absorbed from the diet or synthesized in the liver [37]. However, taurine is also produced as a byproduct of the deconjugation of bile salts via bile salt hydrolases (BSHs) present in the anaerobic gut taxa *Lactobacillus* and *Clostridium* [22]. We

observed increased expression of genes encoding BSH enzymes between days 12 and 86. Given that increased expression of BSH genes corresponded to the beginning of active decomposition, when decomposition products were observed to enter the soil, and the period of reduced dissolved oxygen in our study, it is likely that taurine accumulation is the result of BSH enzyme activity by anaerobic microorganisms. While we did not measure taurine concentrations in the present study, our results correspond to previous decomposition studies that report accumulation of taurine in various organs and body regions [38–40] and soils [18, 41] during decomposition via metabolomics, and increased relative abundance of *Clostridium* and *Lactobacillus* within the body [42–44] and in decomposition soils [20] via DNA sequencing methods, including in these soils [13].

Taurine can be metabolised through desulfurization via the α-ketoglutarate-dependent enzyme taurine dioxygenase (TauD). Specifically, this enzyme, encoded by the gene *tauD*, converts 2-oxoglutarate and taurine to produce aminoacetaldehyde, succinate, sulfite, and CO_2 [45]. Succinate and sulfite from this reaction can then be used for the citric acid cycle and sulfur metabolism, respectively. Given increased BSH expression in our study and reported taurine accumulation in others, we would expect taurine to be present for microbial metabolism by TauD. However, we observed a general decrease in *tauD* expression between days 12 through 376. This trend was driven by reduced expression of *tauD* transcripts associated with *Proteobacteria*, *Gammaproteobacteria*, and *Actinobacteria* whose relative abundance have been shown to remain consistent or increase during human decomposition [20], suggesting that *tauD* expression is downregulated under decomposition conditions. However, we noted that expression of *tauD* genes associated with fungi and a few *Betaproteobacteria* displayed increased representation at day 58, corresponding to increased expression of bile salt hydrolases (BSH) between days 12 and 86. The reduction in *tauD* expression may be due to increased sulfur availability. We did not measure sulfur species

in this experiment; however, others have observed increased sulfur concentrations in decomposition-impacted soils [3, 7, 11]. Thus, sulfur scavenging pathways such as taurine desulfurization by TauD [46], whose genes are expressed under sulfur-limiting conditions, likely display reduced expression under sulfur replete conditions. Additionally, taurine may be processed through other pathways. For example, taurine can be deaminated by taurine dehydrogenase to produce sulfite and acetyl-CoA for carbon metabolism [45, 47]. Overall, our results suggest that human decomposition has potential impacts on soil sulfur biogeochemistry through deposition of inorganic (sulfate) and organic (sulfur-containing amino acids) sulfur compounds.

Conclusion

This study investigated soil microbial gene expression during human decomposition. Metatranscriptomic analysis of soils from three human individuals shows that decomposition impacted microbial community gene expression profiles, exhibiting functional shifts over time for over one year. This included altered expression of genes involved in lipid, N and S metabolism as microbes processed the nutrient-rich tissues of the human body. Additionally, we noted that functionality within decomposition-impacted soils was still affected after one year and had not returned to starting or background conditions. Together, these results show that vertebrate decomposition has lasting impacts on local soil ecosystems, including soil microbial communities. These results have important implications for understanding biogeochemical changes due to vertebrate mortality events in terrestrial ecosystems.

Materials and Methods

Study design

In February 2018, three deceased male human subjects (hereafter, "donors") were placed supine on the soil surface at the University of Tennessee Anthropology Research Facility (ARF) and allowed to decompose. Located in Knoxville, TN (35° 56' 28" N, 83° 56' 25" W) the ARF is a roughly 2-acre outdoor facility dedicated to studying human decomposition [48]. The soils at the ARF are comprised of the Loyston-Talbott-Rock outcrop (LtD) and Coghill-Corryton (CcD) complexes. LtD soils are a silty clay loam and channery clay overlaying lithic bedrock, while CcD soils are comprised of clay from weathered quartz limestone [13, 48]. A site that had not been previously exposed to decomposition was used for this study.

The decomposition field experiment is fully described in Taylor et al. (2024) [13]. Briefly, experiments were conducted in a block design, where each block consisted of one decomposition site and one control site [13]. In total three blocks, *i.e.*, three donors paired with three respective control sites, were included in the study. Each control site was chosen in a manner to ensure their location was uphill and roughly 2 m away from decomposition sites [13]. Donor internal temperatures were recorded by probes located in the abdomen, while ambient air temperatures were monitored via sensors located roughly 50 cm above the soil surface. Soil temperature and salinity were measured with sensors placed directly underneath each individual (Decagon Devices, GS3) [13]. Donor ages ranged from 65 to 86 and were within 1 kg of each other with regard to weight (90.7 to 91.6 kg); donor BMI varied between 27.7 to 29.6 [13].

Sampling and physiochemistry

Decomposition of all subjects was observed for one year. During the one-year study period, soils were sampled at 20 timepoints chosen to correspond with morphological

stages of decomposition as described by [49]. Once advanced decay was reached, soils were collected at intervals of 350 accumulated degree days (ADD), calculated using ambient air temperatures, up to one year. All soil cores were taken using a 1.9 cm (3/4 inch) diameter soil auger to a depth of 16 cm. Soils were divided into two depth fractions: 0-1 cm (interface) and 1-16 cm (core) for the analyses reported in Taylor et al. (2024) [13]; the entire 0 to 16 cm core was used for this current study. Decomposition soils were taken from directly beneath the cadavers, taking care to not re-sample the same location more than once. At the time of sampling, soil dissolved oxygen was measured in triplicate using an Orion Star™ A329 pH/ISE/Conductivity/Dissolved Oxygen portable multiparameter meter (ThermoFisher) [13].

A subset of 6 study timepoints were chosen for metatranscriptomics analysis. Study days 0, 12, 58, 86, 168, and 376 were chosen as they represented distinct morphological and soil biogeochemical stages during decomposition. Study day 0 was chosen as a baseline sample prior to cadaver placement. Study day 12 was the start of active decomposition and corresponded to maximum soil ammonium concentrations and minimum soil oxygen (approximately 39%). Study day 58 was chosen as this sample represented the pH minimum, and respiration and soil temperature were at a maximum [13]. Additionally, ammonium concentrations began to decrease around day 58. Study day 86 was when soil oxygen started to recover and nitrate levels began to increase. Study day 168 was chosen as nitrate was at its maximum and soil dissolved oxygen had returned to 99%. Finally, day 376 was chosen to represent the end of the study, 1 year since cadaver placement. Each study day was represented by four soil samples for RNA extraction: one pooled control sample which was a mix of the three control locations, plus one sample from each of the three donors, yielding a total of 24 samples for this study.

Soil samples were transported back to the University of Tennessee (Knoxville, TN) and processed within 24 hours of collection. Soils were homogenized by hand to remove insect larvae, roots, rocks, and other debris (> 2 mm). A subset of soils were used to measure pH, electrical conductivity (EC), and evolved CO_2 as described in Taylor (2024). Soil nitrogen species (NH_4^+, NO_3^-) and total carbon (TC) and nitrogen (TN) were measured in all soil samples as described in [13]. Reported values for soil physiochemistry represent the full 16 cm core; estimated by summing interface and core values reported by Taylor et. al, (2024) [13] in 1:16 and 15:16 ratios, respectively. Control reported here are means of the three experimental controls that were unimpacted by decomposition.

Roughly 10 g of soil was reserved for nucleic acid extraction, placed in a 4 oz. Whirl-Pak™ bag (Nasco), and flash frozen in liquid nitrogen. All samples were stored at -80°C until further analysis. Bacterial and fungal community composition was assessed via amplicon sequencing of the 16S rRNA gene and ITS2 region as described in Taylor et al. (2024).

RNA Extraction and Sequencing

RNA was extracted from 2 g of soil using Qiagen's RNeasy® PowerSoil® Total RNA kit. Manufacturer's instructions were followed with a few modifications. Soils became saline during decomposition; therefore, we followed the manufacturer's suggestion and incubated all extracts at -20°C following addition of solution SR4 (step 9) to decrease salt precipitation. All RNA samples were resuspended in 40 µl of Solution SR7. RNA concentrations were assessed fluorometrically using the Qubit® RNA HS assay (catalog no. Q32852) with 1 µl of RNA. DNA contamination was removed by DNase treating RNA extracts twice using Qiagen's DNase Max® kit in 50 µl reactions. RNA concentrations were remeasured after DNase treatment. PCR with V4 16S rRNA gene primers [50, 51] was conducted using RNA extracts as the template to confirm removal

of all DNA prior to sequencing. RNA aliquots were shipped to HudsonAlpha Discovery (Huntsville, AL) for library preparation and RNA sequencing. Dual-indexed libraries were prepared using the Illumina® Stranded Total RNA prep with ribosomal RNA depletion via ligation with Ribo-Zero Plus. Libraries were then pooled and sequenced on Illumina's NovaSeq 6000 v4 platform, resulting in demultiplexed fastq files for each sample.

Bioinformatics

Illumina sequencing of the 24 libraries yielded a total of 5,073,476,730 reads, or 2,536,738,365 paired reads, with a mean of 105,697,432 paired reads per sample. Read quality control (QC) was conducted in KBase [52] using Trimmomatic [53]. Paired fastq files were imported to KBase through Globus. Poor quality reads were removed (4.7% of all reads), and adapters trimmed via Trimmomatic (v0.36) using default settings and the TruSeq3-PE-2 adapter file, resulting in 4,834,123,062 total reads. After QC check with FastQC, trimmed libraries were exported as fastq files from KBase through Globus. Remaining ribosomal RNA was filtered using bbmap (maxindel = 20, minid = 0.93) from the Joint Genome Institute's (JGI) bbtools suite [54]. Filtering of ribosomal RNA further removed 7.3% of reads, leaving 4,479,804,360 reads for assembly. Following this step, all non-ribosomal reads from all 24 samples were merged into one file. Reads were then co-assembled into contigs using the de novo assembler MEGAHIT (v1.2.9) [55] (–12 –k-min 23, –k-max 123, –k-step 10).

Gene identification and annotation from co-assembled contigs was performed using Prodigal [56] and eggNOG mapper [57], respectively. Briefly, the DNA fasta containing all contigs was submitted to Prodigal (v2.6.3) for protein coding gene predication for a meta-sample (-p meta -f gff). After co-assembly, a total of 6,257,674 gene calls were identified by Prodigal. Next, predicated genes were functionally and taxonomically annotated using eggNOG mapper (v2.1.6) using basic settings to perform a

diamond blastp search [58]. From this, 1,048,573 proteins were annotated by eggNOG-mapper (16.7%). Most of the annotated proteins were taxonomically annotated as bacteria (91.3%), followed by eukaryotes (7.6 %), and archaea (0.81 %). Of the 7.6% of eukaryotic proteins, 64.4% (4.9% of all proteins) were annotated as fungi. For this study, genes of interest included all bacterial, archaeal, and fungal proteins, therefore all non-fungal eukaryotic proteins (32,004) were removed prior to downstream analysis. Transcript counts for all genes of interest were obtained by mapping reads from each respective sample to genes of interest obtained from co-assembly using QIAGEN CLC Genomics Workbench 20.0 (https://digitalinsights.qiagen.com/). The percent of reads mapped to genes of interest ranged from 21% to 38% between samples, with an average of 31% reads mapped. Gene counts were then combined in a single file and used for downstream analyses in R.

Differential Expression

Transcript counts from all samples were combined in a single workable data file and imported into R for differential expression analysis using the R packages edgeR [59] and limma [60] following a modified pipeline by Phipson et al. (2020) [61]. The transcript count table was imported into R and converted to a DGElist object. Genes without sufficient counts for statistical analysis were removed to increase power using the edgeR function filterByExpr(), using study day as the comparison group.

Raw counts were then log2 normalized and gene expression profiles compared via multidimensional scaling (MDS) and hierarchical clustering. Multidimentional scaling (MDS) was conducted using plotMDS() from the limma package to assess differences between samples. MDS values were extracted from the MDS object, and the first two dimensions plotted using ggplot2 [62]. We also assessed the relationship between gene expression profiles and changes in the soil environment using canonical correspondence analysis (CCA). Environmental variables of interest included decomposition time in

accumulated degree hours (ADH) based on ambient temperatures, ADH based on internal gut temperatures, ADH based on soil temperatures, gravimetric moisture, pH, electrical conductivity (EC), dissolved oxygen (DO), CO_2 (µmol gdw^{-1}), NH_4 (mg gdw^{-1}), NO_3 (mg gdw^{-1}), N %, C %, and CN ratio. First, permutational multivariate analysis of variance (PERMANOVA) with adonis() (vegan v2.6.7) [63] was used to identify significant soil parameters. Then the vegan functions cca() and scores() were applied to run the CCA and extract scores, respectively. Scores for the first two dimension were plotted using ggplot2, with loadings extracted from the CCA biplot.

For differential expression analysis, raw filtered reads were normalized using edgeR's trimmed mean of M values (TMM) normalization using the function calcNormFactors(). TMM normalized reads were then log2 transformed using limma's voom() and differential expression assessed. Empirical Bayes shrinkage was used correct to p-values for false discovery rates. The topmost up and down regulated genes for each comparison, determined by log2 fold change and adjusted p-values, were then reported. Expression of certain genes were assessed after performing transcripts per million (TPM) normalization and statistical analyses with a combination of analysis of variance (ANOVA) and post-hoc Tukey tests. ANOVA across all timepoints were applied to hierarchical linear mixed effects models to account for repeated sampling within each donor block.

Data availability

Raw RNA sequence files from the Illumina Novaseq are available at the National Center for Biotechnology Information's (NCBI) Sequence Read Archive (SRA) as a part of BioProject PRJNA1066312 under BioSample accession numbers SAMN45195141-SAMN45195164. Additional datasets supporting the conclusions of this article are available on GitHub.

Code availability

The code used for analysis and to generate figures are available on GitHub.

References

[1] Benninger, L. A., Carter, D. O. & Forbes, S. L. The biochemical alteration of soil beneath a decomposing carcass. *Forensic Science International* **180**, 70–5 (2008).

[2] Towne, E. G. Prairie vegetation and soil nutrient responses to ungulate carcasses. *Oecologia* **122**, 232–239 (2000). URL https://doi.org/10.1007/PL00008851.

[3] DeBruyn, J. M., Keenan, S. W. & Taylor, L. S. From carrion to soil: microbial recycling of animal carcasses. *Trends in Microbiology* (2024). URL https://doi.org/10.1016/j.tim.2024.09.003. Publisher: Elsevier.

[4] Parmenter, R. R. & MacMahon, J. A. Carrion decomposition and nutrient cycling in a semiarid shrub–steppe ecosystem. *Ecological Monographs* **79**, 637–661 (2009).

[5] Macdonald, B. C. T. *et al.* Carrion decomposition causes large and lasting effects on soil amino acid and peptide flux. *Soil Biology and Biochemistry* **69**, 132–140 (2014).

[6] Bump, J. K. *et al.* Ungulate carcasses perforate ecological filters and create biogeochemical hotspots in forest herbaceous layers allowing trees a competitive advantage. *Ecosystems* **12**, 996–1007 (2009).

[7] Aitkenhead-Peterson, J. A., Owings, C. G., Alexander, M. B., Larison, N. & Bytheway, J. A. Mapping the lateral extent of human cadaver decomposition with soil chemistry. *Forensic Science International* **216**, 127–34 (2012).

[8] Keenan, S. W., Schaeffer, S. M., Jin, V. L. & DeBruyn, J. M. Mortality hotspots: nitrogen cycling in forest soils during vertebrate decomposition. *Soil Biology and Biochemistry* **121**, 165–176 (2018).

[9] Fancher, J. P. *et al.* An evaluation of soil chemistry in human cadaver decomposition islands: Potential for estimating postmortem interval (PMI). *Forensic Science International* **279**, 130–139 (2017).

[10] Quaggiotto, M.-M., Evans, M. J., Higgins, A., Strong, C. & Barton, P. S. Dynamic soil nutrient and moisture changes under decomposing vertebrate carcasses. *Biogeochemistry* **146**, 71–82 (2019).

[11] Taylor, L. S. *et al.* Soil elemental changes during human decomposition. *PLoS ONE* **18**, 1–24 (2023). URL https://doi.org/10.1371/journal.pone.0287094. Publisher: Public Library of Science.

[12] Mason, A. R. *et al.* Body mass index (BMI) impacts soil chemical and microbial response to human decomposition. *mSphere* e0032522 (2022).

[13] Taylor, L. S. *et al.* Transient hypoxia drives soil microbial community dynamics and biogeochemistry during human decomposition. *FEMS Microbiology Ecology* **100**, fiae119 (2024). URL https://doi.org/10.1093/femsec/fiae119.

[14] Keenan, S. W., Emmons, A. L. & DeBruyn, J. M. Microbial community coalescence and nitrogen cycling in simulated mortality decomposition hotspots. *Ecological Processes* **12**, 45 (2023). URL https://doi.org/10.1186/s13717-023-00451-y.

[15] Mason, A. R., Taylor, L. S. & DeBruyn, J. M. Microbial ecology of vertebrate decomposition in terrestrial ecosystems. *FEMS Microbiology Ecology* **99**, fiad006 (2023). URL https://doi.org/10.1093/femsec/fiad006.

[16] Burcham, Z. M. *et al.* Total RNA analysis of bacterial community structural and functional shifts throughout vertebrate decomposition. *Journal of Forensic Sciences* **64**, 1707–1719 (2019).

[17] Ashe, E. C., Comeau, A. M., Zejdlik, K. & O'Connell, S. P. Characterization of bacterial community dynamics of the human mouth throughout decomposition via metagenomic, metatranscriptomic, and culturing techniques. *Frontiers in Microbiology* **12**, 689493 (2021).

[18] DeBruyn, J. M. *et al.* Comparative decomposition of humans and pigs: soil biogeochemistry, microbial activity and metabolomic profiles. *Frontiers in Microbiology* **11**, 608856 (2021).

[19] Howard, G. T., Duos, B. & Watson-Horzelski, E. J. Characterization of the soil microbial community associated with the decomposition of a swine carcass. *International Biodeterioration & Biodegradation* **64**, 300–304 (2010).

[20] Cobaugh, K. L., Schaeffer, S. M. & DeBruyn, J. M. Functional and structural succession of soil microbial communities below decomposing human cadavers. *Plos One* **10**, e0130201 (2015).

[21] Singh, B. *et al.* Temporal and spatial impact of human cadaver decomposition on soil bacterial and arthropod community structure and function. *Frontiers in Microbiology* **8**, 2616 (2018).

[22] Urdaneta, V. & Casadesús, J. Interactions between Bacteria and Bile Salts in the Gastrointestinal and Hepatobiliary Tracts. *Frontiers in Medicine* **4** (2017).

[23] van der Wal, A., Geydan, T. D., Kuyper, T. W. & de Boer, W. A thready affair: linking fungal diversity and community dynamics to terrestrial decomposition processes. *FEMS Microbiology Reviews* **37**, 477–494 (2013).

[24] Essington, M. E. *Soil and water chemistry: an integrative approach* (CRC press, 2015).

[25] Peng, J., Wegner, C.-E. & Liesack, W. Short-term exposure of paddy soil microbial communities to salt stress triggers different transcriptional responses of key taxonomic groups. *Frontiers in Microbiology* **8** (2017).

[26] Pandit, A. S. *et al.* A snapshot of microbial communities from the Kutch: one of the largest salt deserts in the World. *Extremophiles* **19**, 973–987 (2015).

[27] Metcalf, J. L. *et al.* Microbial community assembly and metabolic function during mammalian corpse decomposition. *Science* **351**, 158–62 (2016).

[28] Fu, X. *et al.* Fungal succession during mammalian cadaver decomposition and potential forensic implications. *Scientific Reports* **9**, 12907 (2019).

[29] Dujon, B. *et al.* Genome evolution in yeasts. *Nature* **430**, 35–44 (2004).

[30] Haridas, S. *et al.* The genome and transcriptome of the pine saprophyte Ophiostoma piceae, and a comparison with the bark beetle-associated pine pathogen Grosmannia clavigera. *BMC Genomics* **14**, 373 (2013).

[31] Notter, S. J., Stuart, B. H., Rowe, R. & Langlois, N. The initial changes of fat deposits during the decomposition of human and pig remains. *Journal of Forensic Sciences* **54**, 195–201 (2009).

[32] Kok, R. G. *et al.* Characterization of the extracellular lipase, LipA, of Acinetobacter calcoaceticus BD413 and sequence analysis of the cloned structural gene. *Molecular Microbiology* **15**, 803–818 (1995).

[33] Hasan, F., Shah, A. A. & Hameed, A. Influence of culture conditions on lipase production by Bacillus sp. FH5. *Annals of Microbiology* **56**, 247–252 (2006).

[34] Zouaoui, B. & Bouziane, A. Production, optimization and characterization of the lipase from Pseudomonas aeruginosa. *Romanian biotechnological letters* **17**, 7187–7193 (2012).

[35] Soler-Jofra, A., Pérez, J. & van Loosdrecht, M. C. M. Hydroxylamine and the nitrogen cycle: A review. *Water Research* **190**, 116723 (2021).

[36] Yu, R., Perez-Garcia, O., Lu, H. & Chandran, K. Nitrosomonas europaea adaptation to anoxic-oxic cycling: Insights from transcription analysis, proteomics and metabolic network modeling. *Science of the Total Environment* **615**, 1566–1573 (2018).

[37] Seidel, U., Huebbe, P. & Rimbach, G. Taurine: A regulator of cellular redox homeostasis and skeletal muscle function. *Molecular Nutrition & Food Research* **63**, 1800569 (2019).

[38] Mora-Ortiz, M., Trichard, M., Oregioni, A. & Claus, S. P. Thanatometabolomics: introducing NMR-based metabolomics to identify metabolic biomarkers of the time of death. *Metabolomics* **15**, 37 (2019).

[39] Locci, E. *et al.* A 1H NMR metabolomic approach for the estimation of the time since death using aqueous humour: an animal model. *Metabolomics* **15**, 76 (2019).

[40] Zelentsova, E. A. *et al.* Post-mortem changes in the metabolomic compositions of rabbit blood, aqueous and vitreous humors. *Metabolomics* **12**, 172 (2016).

[41] Hoeland Katharina, M. *Investigating the potential of postmortem metabolomics in mammalian decomposition studies in outdoor settings.* Ph.D. thesis, University of Tennessee-Knoxville, https://trace.tennessee.edu/utk_graddiss/7000 (2021).

[42] Javan, G. T. *et al.* Human thanatomicrobiome succession and time since death. *Scientific Reports* **6**, 29598 (2016).

[43] Javan, G. T., Finley, S. J., Smith, T., Miller, J. & Wilkinson, J. E. Cadaver thanatomicrobiome signatures: the ubiquitous nature of Clostridium species in human decomposition. *Frontiers in Microbiology* **8**, 2096 (2017).

[44] DeBruyn, J. M. & Hauther, K. A. Postmortem succession of gut microbial communities in deceased human subjects. *Peerj* **5**, e3437 (2017).

[45] Cook, A. M. & Denger, K. Metabolism of taurine in microorganisms. *Taurine 6* 3–13 (2006).

[46] Kertesz, M. A. Riding the sulfur cycle – metabolism of sulfonates and sulfate esters in Gram-negative bacteria. *FEMS Microbiology Reviews* **24**, 135–175 (2000).

[47] Brüggemann, C., Denger, K., Cook, A. M. & Ruff, J. Enzymes and genes of taurine and isethionate dissimilation in Paracoccus denitrificans. *Microbiology (Reading, England)* **150**, 805–816 (2004).

[48] Keenan, S. W. *et al.* Spatial impacts of a multi-individual grave on microbial and microfaunal communities and soil biogeochemistry. *PLoS One* **13**, e0208845 (2018).

[49] Payne, J. A. A summer carrion study of the baby pig Sus Scrofa Linnaeus. *Ecology* **46**, 592–602 (1965).

[50] Apprill, A., McNally, S., Parsons, R. & Weber, L. Minor revision to V4 region SSU rRNA 806R gene primer greatly increases detection of SAR11 bacterioplankton. *Aquatic Microbial Ecology* **75**, 129–137 (2015).

[51] Parada, A. E., Needham, D. M. & Fuhrman, J. A. Every base matters: assessing small subunit rRNA primers for marine microbiomes with mock communities, time series and global field samples. *Environmental Microbiology* **18**, 1403–14 (2016).

[52] Arkin, A. P. *et al.* KBase: The United States Department of Energy Systems Biology Knowledgebase. *Nature Biotechnology* **36**, 566–569 (2018).

[53] Bolger, A. M., Lohse, M. & Usadel, B. Trimmomatic: a flexible trimmer for Illumina sequence data. *Bioinformatics* **30**, 2114–2120 (2014).

[54] Bushnell, B. Bbtools software packag. *e* (2014).

[55] Li, D., Liu, C.-M., Luo, R., Sadakane, K. & Lam, T.-W. MEGAHIT: an ultra-fast single-node solution for large and complex metagenomics assembly via succinct de Bruijn graph. *Bioinformatics* **31**, 1674–1676 (2015).

[56] Hyatt, D. *et al.* Prodigal: prokaryotic gene recognition and translation initiation site identification. *BMC Bioinformatics* **11**, 119 (2010).

[57] Cantalapiedra, C. P., Hernández-Plaza, A., Letunic, I., Bork, P. & Huerta-Cepas, J. eggNOG-mapper v2: functional annotation, orthology assignments, and domain prediction at the metagenomic scale. *Molecular Biology and Evolution* **38**, 5825–5829 (2021).

[58] Buchfink, B., Reuter, K. & Drost, H.-G. Sensitive protein alignments at tree-of-life scale using DIAMOND. *Nature Methods* **18**, 366–368 (2021).

[59] Robinson, M. D., McCarthy, D. J. & Smyth, G. K. edgeR: a Bioconductor package for differential expression analysis of digital gene expression data. *Bioinformatics* **26**, 139–140 (2010).

[60] Smyth, G. K. in *limma: Linear Models for Microarray Data* (eds Gentleman, R., Carey, V. J., Huber, W., Irizarry, R. A. & Dudoit, S.) *Bioinformatics and Computational Biology Solutions Using R and Bioconductor* 397–420 (Springer New York, New York, NY, 2005).

[61] Phipson, B. *et al.* Differential expression analysis (2020). URL https://combine-australia.github.io/RNAseq-R/06-rnaseq-day1.html#References.

[62] Wickham, H. *ggplot2: Elegant Graphics for Data Analysis* (Springer-Verlag New York, 2016). URL https://ggplot2.tidyverse.org.

[63] Oksanen, J. *et al.* *vegan: Community Ecology Package* (2024). URL https://vegandevs.github.io/vegan/.

Figures

Figure 1: **Microbial gene expression profiles are altered during human decomposition.** Multidimensional scaling (MDS) shows gene expression within soils changed as decomposition progressed (A). Additionally, canonical correspondence analysis (CCA) shows that environmental variables explained 47.3% of the variation in gene expression profiles (B). Variables in bold red type significantly ($p < 0.05$) explained some of the variation in gene expression profiles as assessed by Permutational Analysis of Variance (PERMANOVA). In both panels soils from controls (CON) and the three donors (SP1, SP2, SP3) are denoted by symbol shape, while color represents study day. In B, soil physiochemical variable loadings are represented by arrows: Gravimetric water content (GWC), electrical conductivity (EC), pH (pH), dissolved oxygen (DO), respiration (evolved CO_2 µmol gdw^{-1}), ammonium (NH_4), and nitrate (NO_3) concentrations (mg gdw^{-1}), percent carbon (%C), percent nitrogen (%N), carbon:nitrogen ratio (C:N), ambient temperature (T_A), and soil temperature (T_S).

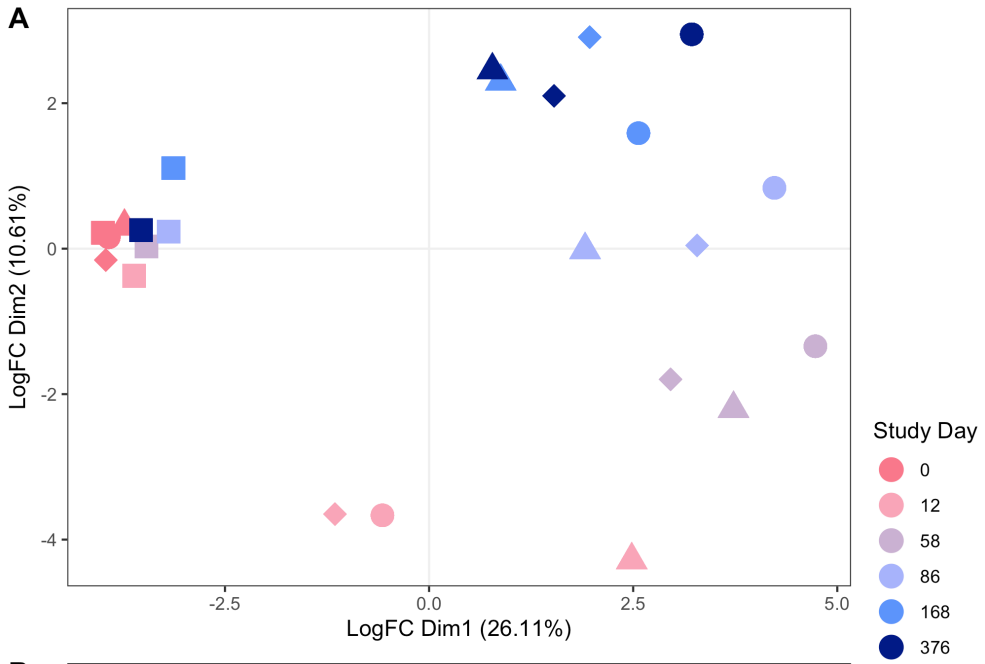
A
LogFC Dim2 (10.61%)
LogFC Dim1 (26.11%)
2
0
-2
-4
-2.5
0.0
2.5
5.0
Study Day
0
12
58
86
168
376

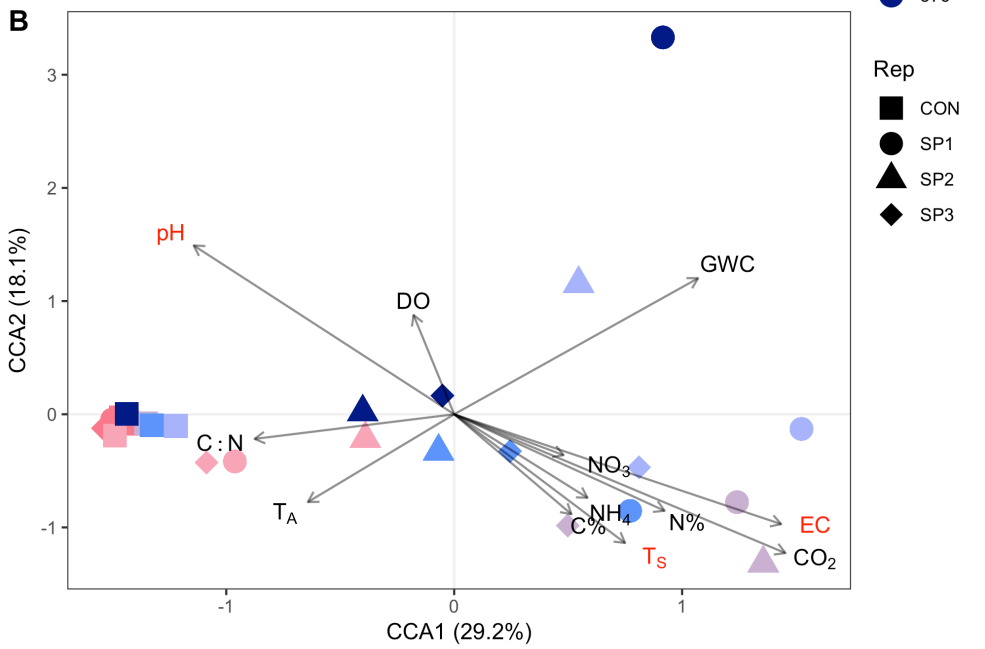
B
CCA2 (18.1%)
CCA1 (29.2%)
3
2
1
0
-1
-1
0
1
pH
GWC
DO
C : N
T_A
NO_3
NH_4
C%
N%
EC
T_S
CO_2
Rep
CON
SP1
SP2
SP3

Figure 2: **Mean normalized log2 expression of heat shock proteins identified by differential expression analysis comparing decomposition and control soils.** Each panel represents a single heat shock gene, labeled with gene names, identified via Prodigal. Symbol color denotes if the sample is a control (CON, green), or one of three individuals: SP1 (orange), SP2 (purple), or SP3 (pink). Error bars are standard error of individual query genes in the top 20 transcripts associated with decomposition soils.

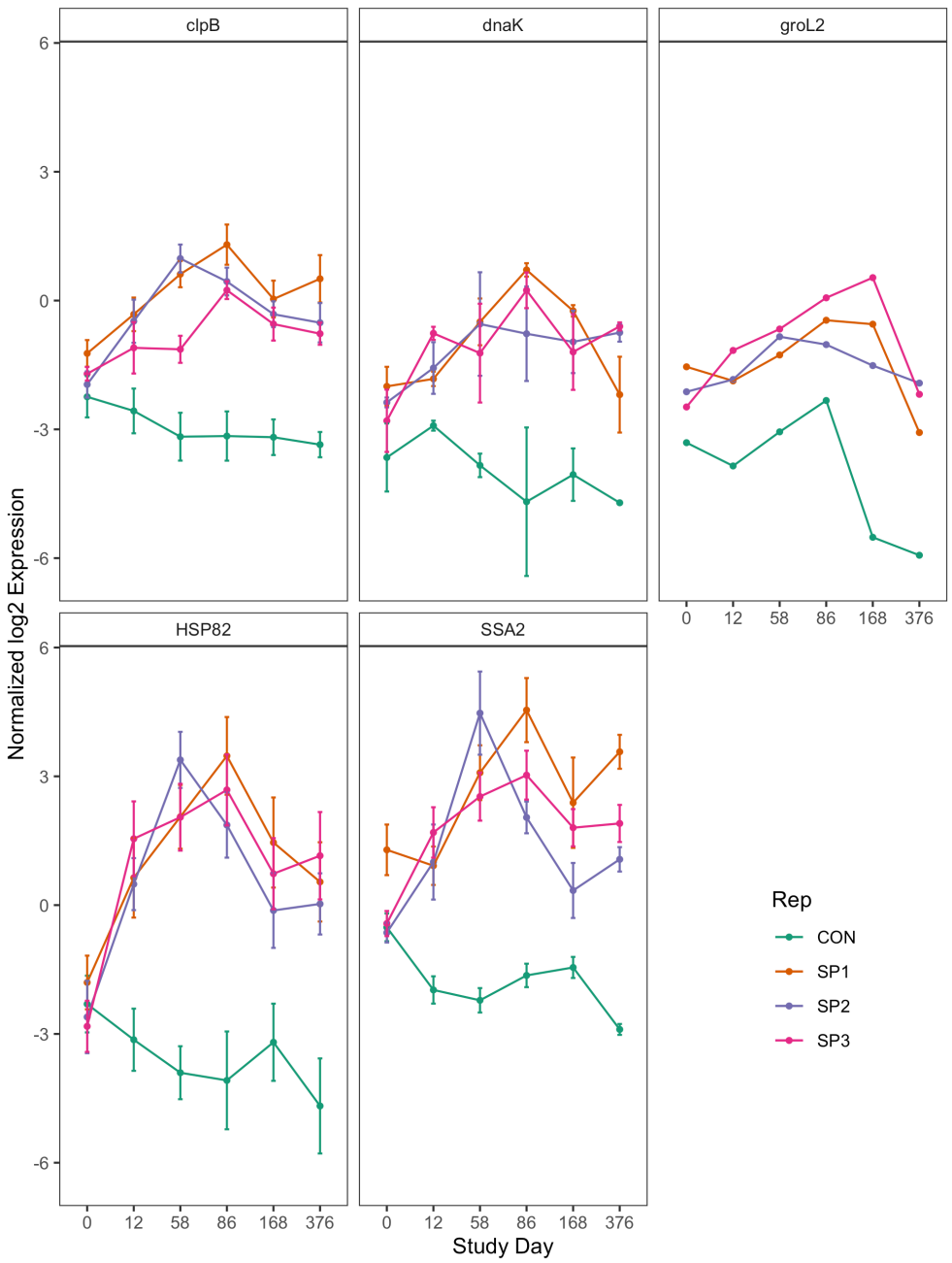
clpB
dnaK
groL2
HSP82
SSA2
Normalized log2 Expression
6
3
0
-3
-6
0
12
58
86
168
376
Study Day
Rep
CON
SP1
SP2
SP3

Figure 3: **Top twenty up- and down-regulated genes in decomposition soils comparing sequential study days (0, 12, 58, 86, 168, 376) colored by COG functional category (A) and taxonomic annotation (B).** Positive values denote increased expression compared to the preceding timepoint, while negative values denote a decrease.

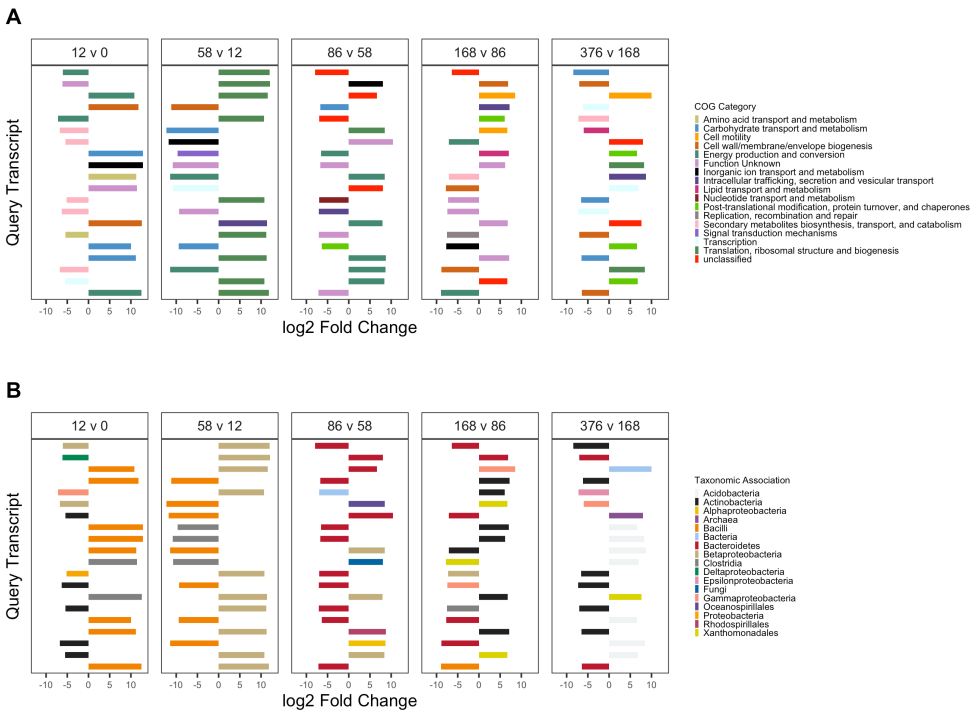

Figure 4: **Mean transcript abundance, in transcripts per million (TPM), of all bacterial (A) and fungal (B) triacylglycerol lipase (EC 3.1.1.3) genes over time.** Abundance of both bacterial (Anova p = 0.001) and fungal (Anova p = 0.015) lipase transcripts change significantly over time. Black lines (A, B) report mean and standard deviation of TPM from three individuals (black line), while gold stars denote mean TPM in control soils. Letters are the result of post-hoc Tukey tests between decomposition timepoints. In B, bars show the relative abundance of the fungal classes *Saccharomycetes*, *Sordariomycetes*, and *Eurotiomycetes*, reported in Taylor et al. (2024).

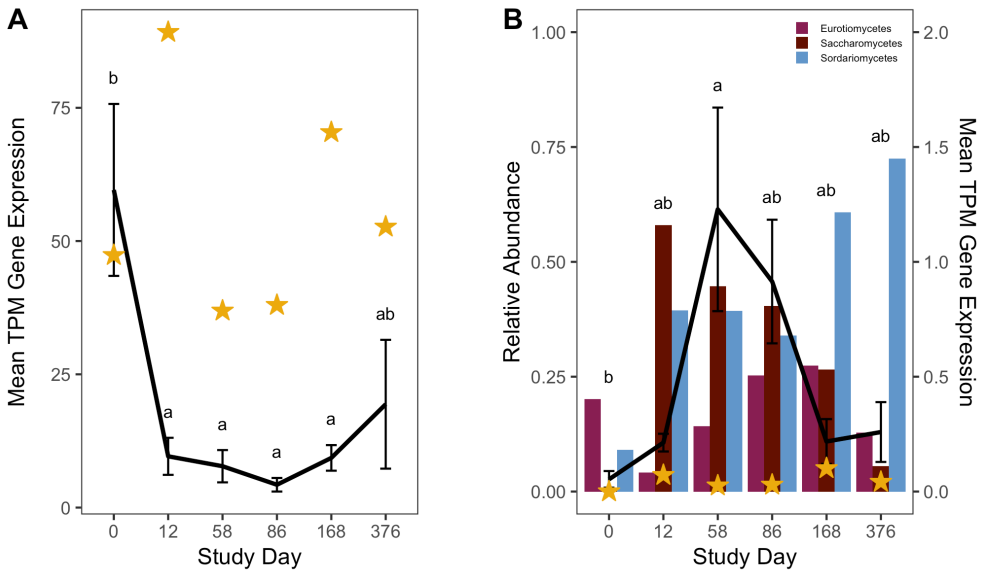

Figure 5: **Mean gene expression, in transcripts per million (TPM), of commonly used marker genes for enzymes involved in nitrogen cycling over time in controls (A) and decomposition (B) soils.** Data in B represent mean and standard deviation of TPM from three individuals.

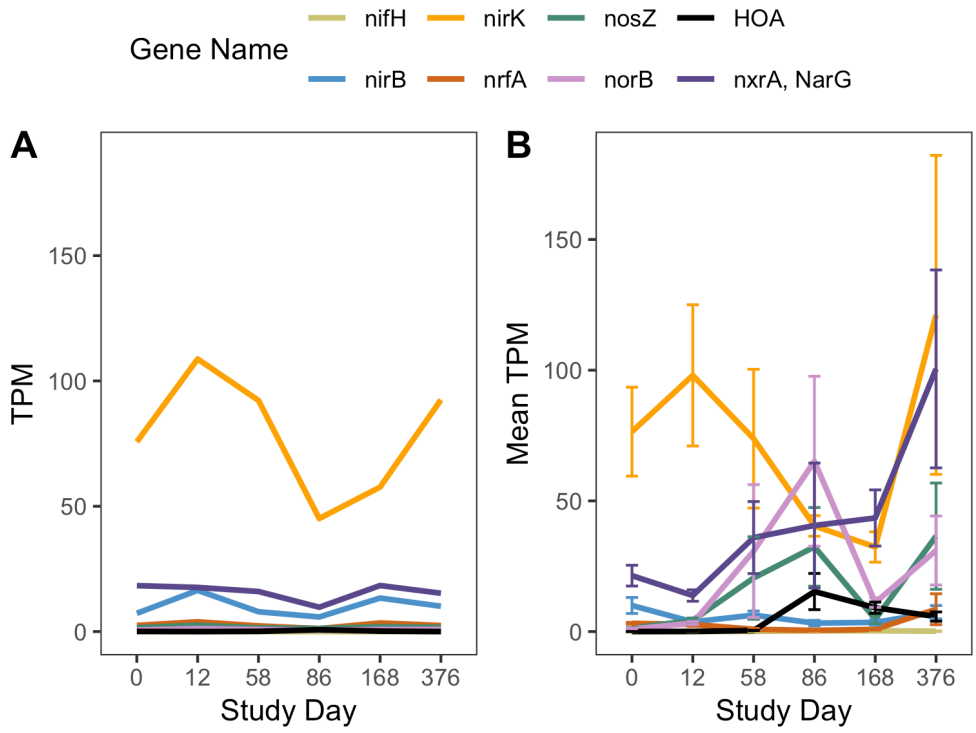

Figure 6: **Mean bile salt hydrolase, BSH, (A) and *tauD*, taurine dioxygenase, (B) log2 normalized expression in controls (gold stars) and decomposition (boxplots) soils.** Boxplots display the 25th and 75th quartiles and median log2 normalized values between all three individuals at each timepoint. ANOVA p-value is the result of a hierarchical linear mixed effects model accounting for repeated measures of each donor block, while letters denote the results of *post-hoc* Tukey test.

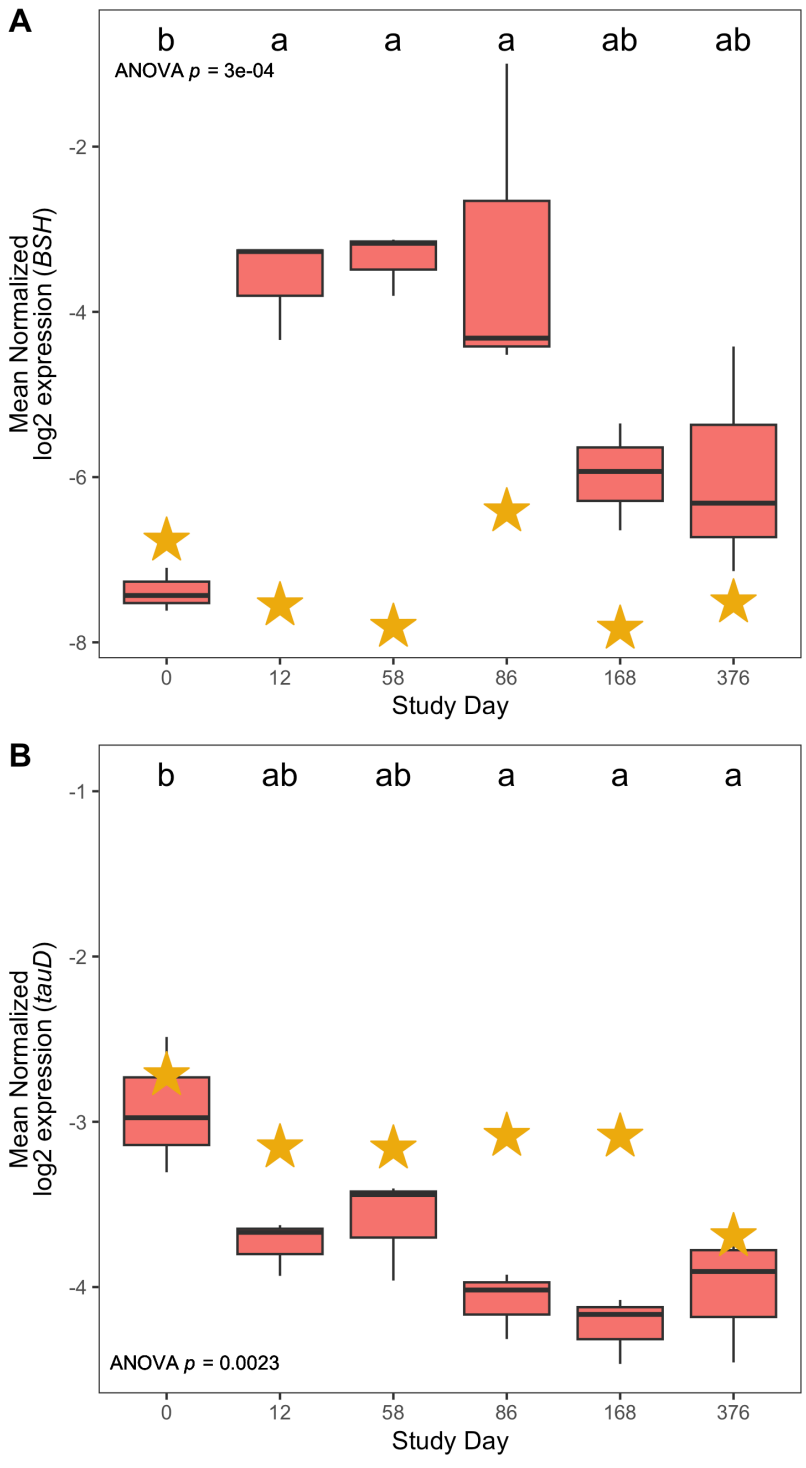
A
b
a
a
a
ab
ab
ANOVA p = 3e-04
Mean Normalized log2 expression (BSH)
-2
-4
-6
-8
0
12
58
86
168
376
Study Day
B
b
ab
ab
a
a
a
-1
-2
-3
-4
ANOVA p = 0.0023
Mean Normalized log2 expression (tauD)
0
12
58
86
168
376
Study Day

Acknowledgements

We would like to thank the Forensic Anthropology Center at the University of Tennessee-Knoxville for their help in setting up field experiments. We would like to thank Mary Davis for her help in managing the field site and helping to obtain donors for this work. This research was funded by a National Institute of Justice Award (DOJ-NIJ-2017-R2-CX-0008) to LST and JMD.